

# Pressure-induced superconductivity in topological insulator $\text{Ge}_2\text{Bi}_2\text{Te}_5$ and the evolution with Mn doping

Shangjie Tian<sup>1,2,3,†</sup>, Qi Wang<sup>4,5,†</sup>, Yuqing Cao<sup>2,3</sup>, Ying Ma<sup>6</sup>, Xiao Zhang<sup>6,\*</sup>, Yanpeng Qi<sup>4,5,7,\*</sup>, Hechang Lei<sup>2,3,\*</sup>, and Shouguo Wang<sup>1,\*</sup>

<sup>1</sup>*Anhui Provincial Key Laboratory of Magnetic Functional Materials and Devices,*

*School of Materials Science and Engineering, Anhui University, Hefei 230601, China*

<sup>2</sup>*School of Physics and Beijing Key Laboratory of Optoelectronic Functional Materials & MicroNano Devices,  
Renmin University of China, Beijing 100872, China*

<sup>3</sup>*Key Laboratory of Quantum State Construction and Manipulation (Ministry of Education),  
Renmin University of China, Beijing 100872, China*

<sup>4</sup>*State Key Laboratory of Quantum Functional Materials,  
School of Physical Science and Technology, ShanghaiTech University, Shanghai 201210, China*

<sup>5</sup>*ShanghaiTech Laboratory for Topological Physics,  
ShanghaiTech University, Shanghai 201210, China*

<sup>6</sup>*State Key Laboratory of Information Photonics and Optical Communications & School of Physical Science and Technology,  
Beijing University of Posts and Telecommunications, Beijing 100876, China*

<sup>7</sup>*Shanghai Key Laboratory of High-resolution Electron Microscopy,  
ShanghaiTech University, Shanghai 201210, China*

(Dated: January 26, 2026)

Introducing superconductivity (SC) or magnetism into topological insulators (TIs) can give rise to novel quantum states and exotic physical phenomena. Here, we report a high-pressure transport study on the TI  $\text{Ge}_2\text{Bi}_2\text{Te}_5$  and its Mn-doped counterparts. The application of pressure induces a SC in  $\text{Ge}_2\text{Bi}_2\text{Te}_5$ , which shows a dome-shape phase diagram with the maximum  $T_c$  of 7.6 K at 23 GPa. Doping Mn into  $\text{Ge}_2\text{Bi}_2\text{Te}_5$  introduces an antiferromagnetic order at ambient pressure and strongly weakens the pressure-induced SC, demonstrating that magnetism and SC compete in this material system. Present study provides a new platform for investigating the interplay among band topology, magnetism, and SC.

## I. INTRODUCTION

Following the theoretical prediction and experimental confirmation of topological insulators (TIs), significant research interest has expanded to a broad class of materials exhibiting nontrivial band topology [1–5]. TIs are characterized by an insulating bulk state with robust, gapless surface states (SSs) protected by time-reversal symmetry [1–3]. The interplay of topology with magnetism or superconductivity (SC) leads to even richer exotic phenomena. For instance, when magnetism is introduced into a TI, it breaks time-reversal symmetry. This opens a gap in the SS and gives rise to dissipationless quantized edge transport [6–12]. Therefore, magnetic TIs (MTIs) can host a set of emergent phenomena such as quantum anomalous Hall effect, axion insulating state, and quantum magnetoelectric effect [6–13]. Similarly, engineering SC in topological materials is generally believed to be an effective approach to achieving topological SC (TSC), which can support Majorana fermions at the edge states and Majorana zero mode at vortex cores, which are potentially useful in topological quantum computing [14–22]. Despite theoretical advances indicating that over half of known materials may possess nontrivial band topology [23–25], only a very limited number of materials exhibit either intrinsic magnetism or SC. This scarcity hinders the search for intrinsic MTI or TSC. The exploration of new magnetic or superconductive materials with topological band structures remains a prominent

and challenging frontier in condensed matter physics.

The layered pseudobinary chalcogenides  $mAX \cdot nB_2X_3$  ( $A = \text{Ge}, \text{Sn}, \text{Pb}, \text{Mn}; B = \text{Sb}, \text{Bi}; X = \text{Se}, \text{Te}; m = 0, n = 1$  or  $m = 1, n \geq 1$  or  $m \geq 2, n = 1$ ) have attracted extensive research interest due to their nontrivial band topology which host exotic topological physical properties [13, 26–47]. Moreover, SC has also been widely explored in this material family. For example, pressurized  $\text{Bi}_2\text{Se}_3$  and  $\text{Bi}_2\text{Te}_3$  become bulk superconductors with transition temperature  $T_c$  up to  $\sim 7$  K [48, 49]. Chemical pressure induced by In doping in  $\text{SnBi}_2\text{Te}_4$  and  $\text{PbBi}_2\text{Te}_4$  also leads to SC near 2 K [50, 51]. Moreover, several nonmagnetic members—including  $\text{GeBi}_2\text{Te}_4$ ,  $\text{GeBi}_4\text{Te}_7$ ,  $\text{GeSb}_2\text{Te}_4$ ,  $\text{SnBi}_2\text{Te}_4$ , and so on—exhibit pressure-induced SC with maximum  $T_c$  values ranging from 6.3 to 8.5 K [52–57]. In contrast, among magnetic members, SC remains scarce, with  $\text{MnSb}_4\text{Te}_7$  being the only example reported so far, showing a low  $T_c$  of about 2 K at 50 GPa [58].

Theoretical predicts that  $\text{Ge}_2\text{Bi}_2\text{Te}_5$  is TI with a single Dirac cone [45], which has been confirmed experimentally by our recent work [59]. On the other hand, recent study has reported the successful Mn doping into  $\text{Ge}_2\text{Bi}_2\text{Te}_5$ , although the synthesis of pure  $\text{Mn}_2\text{Bi}_2\text{Te}_5$  remains challenging [60].  $(\text{Ge}_{1-x}\text{Mn}_x)_2\text{Bi}_2\text{Te}_5$  single crystals with  $x$  up to 0.47 can be grown and the  $x = 0.47$  sample shows an antiferromagnetism (AFM) with  $T_N \sim 11$  K [60]. In this work, we carry out a systematic study on electrical transport properties of  $(\text{Ge}_{1-x}\text{Mn}_x)_2\text{Bi}_2\text{Te}_5$  ( $0 \leq x \leq 0.49$ ) under pressure. We discover SC in  $\text{Ge}_2\text{Bi}_2\text{Te}_5$  with

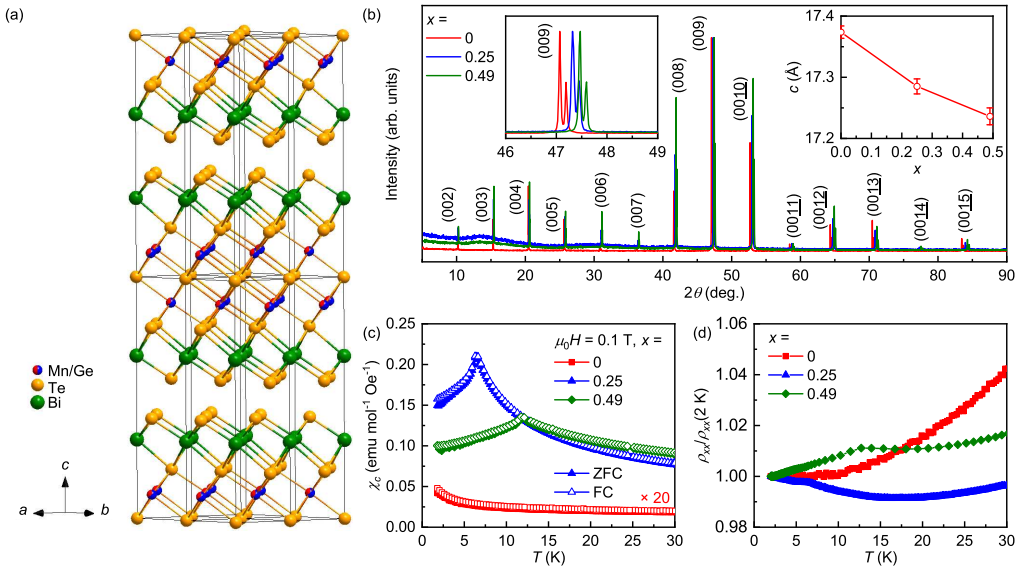


FIG. 1. (a) Structure of  $(\text{Ge}_{1-x}\text{Mn}_x)\text{Bi}_2\text{Te}_5$  single crystal. The red, blue, green and orange balls represent Ge, Mn, Bi and Te atoms, respectively. (b) Single-crystal XRD patterns of  $(\text{Ge}_{1-x}\text{Mn}_x)\text{Bi}_2\text{Te}_5$  single crystals. The left inset shows the enlarged part of (009) peaks. The right inset presents the fitted  $c$ -axial lattice parameter as a function of  $x$ . (c) Temperature dependence of  $\chi_c(T)$  for  $(\text{Ge}_{1-x}\text{Mn}_x)\text{Bi}_2\text{Te}_5$  single crystals under  $0.1$  T with ZFC and FC modes. The curves of  $\text{Ge}_2\text{Bi}_2\text{Te}_5$  are magnified by a factor of 20 for clarity. (d) Normalized resistivity  $\rho_{xx}(T)/\rho_{xx}(2\text{ K})$  as a function of temperature for  $(\text{Ge}_{1-x}\text{Mn}_x)\text{Bi}_2\text{Te}_5$  single crystals.

maximum  $T_c \sim 7.6$  K at  $23.0$  GPa. Furthermore, it is found that Mn doping induces AFM at ambient pressure but suppresses SC quickly under high pressure, implying the competing relationship between AFM and SC in this material series.

## II. METHODS

**Sample synthesis.** Single crystals of  $\text{Ge}_2\text{Bi}_2\text{Te}_5$  were grown by the self-flux method. The high-purity Ge (99.999 %), Bi (99.999 %) and Te (99.999 %) shots were put into corundum crucibles and sealed into quartz tubes with a ratio of Ge : Bi : Te = 2 : 2 : 8. The tube was heated to 1273 K at a rate of 40 K/h and held there for 12 h to ensure a homogeneous melt. Then the temperature was rapidly cooled down to 672 K with subsequently cooling down to 593 K at 1 K/h. The flux is removed by centrifugation, and shiny crystals can be obtained. For Mn-doped single crystals  $(\text{Ge}_{1-x}\text{Mn}_x)\text{Bi}_2\text{Te}_5$ , they are difficult to synthesize by using the flux method, and the chemical vapour transport (CVT) method needs to be used [60]. Ge (99.999 %), Mn (99.9 %), Bi (99.999 %) and Te (99.999 %) powders with the molar ratio of Ge/Mn : Bi : Te = 4 : 2 : 6 were put in a silica tube with a length of 200 mm and an inner diameter of 15 mm. Then, 200 mg  $\text{I}_2$  was added into the tube as a transport reagent. The tube was evacuated to  $10^{-2}$  Pa and sealed under vacuum. The tubes were placed in a two-zone horizontal tube furnace, slowly heated to 1273 K, and held at this temperature for 24 h. Then the temperatures of the

source and growth zones were cooled to 813 K and 793 K, respectively, and held there for two weeks. Shiny crystals with lateral dimensions of up to several millimetres can be obtained.

**Structural and composition characterizations.** The X-ray diffraction (XRD) patterns of  $(\text{Ge}_{1-x}\text{Mn}_x)\text{Bi}_2\text{Te}_5$  single crystals were performed using a Bruker D8 X-ray diffractometer with  $\text{Cu } K_\alpha$  radiation ( $\lambda = 1.5418$  Å) at room temperature. The elemental analysis was performed using energy-dispersive X-ray (EDX) spectroscopy analysis in a FEI Nano 450 scanning electron microscope.

**Transport and magnetization characterizations.** Electrical transport measurements were conducted using a superconducting magnetic system (Cryomagnetics, C-Mag Vari-9). Magnetization measurements were performed using a Quantum Design magnetic property measurement system (MPMS3).

**High Pressure Transport.** *In-situ* high-pressure electrical transport measurements were carried out in the Quantum Design Physical Property Measurement System (PPMS-9T). The van der Pauw method was employed to measure the resistivity. Small pieces of  $(\text{Ge}_{1-x}\text{Mn}_x)\text{Bi}_2\text{Te}_5$  single crystal were loaded into the chamber of diamond anvil cell (DAC) with 200  $\mu\text{m}$ -sized diamond culets. The ruby luminescence at room temperature was utilized to obtain the pressure values within the DAC [61].

### III. RESULTS AND DISCUSSION

As depicted in Fig. 1(a),  $(\text{Ge}_{1-x}\text{Mn}_x)\text{Bi}_2\text{Te}_5$  crystallizes in a layered rhombohedral structure with space group  $P\bar{3}m1$  (No. 164) [60, 62–64], where the fundamental building block is a nonuple layer (NL) with the stacking sequence Te–Bi–Te–Ge/Mn–Te–Ge/Mn–Te–Bi–Te, and these NLs are stacked along the  $c$ -axis via weak vdW interactions. The EDX spectra show that the actual compositions of present crystals are  $\text{Ge}_{1.91(2)}\text{Bi}_{2.11(2)}\text{Te}_5$  (noted as  $x = 0$ ),  $(\text{Ge}_{0.75}\text{Mn}_{0.25})_{1.77(2)}\text{Bi}_{2.18(2)}\text{Te}_5$  ( $x = 0.25$ ), and  $(\text{Ge}_{0.51}\text{Mn}_{0.49})_{1.81(2)}\text{Bi}_{2.17(2)}\text{Te}_5$  ( $x = 0.49$ ) when setting Te content as 5. The deviation from ideal stoichiometry of 2 : 2 : 5 suggests that there are some  $\text{Ge}_{\text{Bi}}$  antisite defects in this series of materials, consistent with previous study [60]. Single-crystal XRD patterns at ambient pressure (Fig. 1(b)) show that all reflections can be indexed to the  $(00l)$  peaks of the trigonal  $P\bar{3}m1$  space group, confirming that the crystallographic  $c$ -axis is perpendicular to the sample surface. Moreover, with increasing Mn content  $x$ , the  $(00l)$  peaks shift systematically to higher angles (left inset of Fig. 1(b)), reflecting a gradual decrease in the  $c$ -axial lattice parameter from 17.37(1) Å ( $x = 0$ ) to 17.29(1) Å ( $x = 0.25$ ) and 17.24(1) Å ( $x = 0.49$ ) (right inset of Fig. 1(b)), consistent with the smaller size of Mn ion than that of Ge ion. The temperature-dependent  $c$ -axial magnetic susceptibility  $\chi_c(T)$  (Figs. 1(c) and S1(a) in the Supplemental Material [65]) reveals antiferromagnetic (AFM) order in the Mn-doped samples. The Néel temperature  $T_N$  increases gradually from 6.0 K to 11.8 K when the  $x$  increases from 0.25 to 0.49, in agreement with the results in the literature [60]. Figures 1(d) and S1(b) [65] shows the temperature dependence of in-plane normalized resistivity  $\rho_{xx}(T)/\rho_{xx}(2 \text{ K})$ . All of  $(\text{Ge}_{1-x}\text{Mn}_x)\text{Bi}_2\text{Te}_5$  crystals show metallic behaviors, i.e., the  $\rho_{xx}(T)$  decreases with cooling from 300 K down to 2 K in general. It is noted that a kink appears in the Mn-doped samples at low-temperature region and the corresponding temperatures are close to the  $T_{\text{NS}}$ , which can be ascribed to the suppression of spin scattering upon entering the AFM state.

Figures 2(a) and 2(b) show the high-pressure transport results of the  $\text{Ge}_2\text{Bi}_2\text{Te}_5$  single crystal. At 0.7 GPa, the  $\rho(T)$  curve shows a metallic behavior in the whole temperature range, which is in line with that under ambient pressure. With increasing pressure, the values of  $\rho(T)$  decrease gradually. Importantly, there is a slight drop in  $\rho(T)$  curve at the onset temperature  $T_{c,\text{onset}} \sim 2.46$  K under a pressure of 3.8 GPa. As the pressure increases to 11.1 GPa, the  $\rho(T)$  curve drops significantly at  $T_{c,\text{onset}} \sim 3.99$  K and reaches zero at  $T_{c,\text{zero}} \sim 1.96$  K. It suggests that such resistivity drop is due to the pressure-induced SC in  $\text{Ge}_2\text{Bi}_2\text{Te}_5$ . Upon further compression, the  $T_{c,\text{onset}}$  initially increases and approaches the maximum value of  $\sim 7.58$  K at 23.0 GPa. Subsequently, the  $T_{c,\text{onset}}$  begins to decrease monotonically under higher pressure. Furthermore, the repeated measurements conducted on another  $\text{Ge}_2\text{Bi}_2\text{Te}_5$  single crystal also exhibit

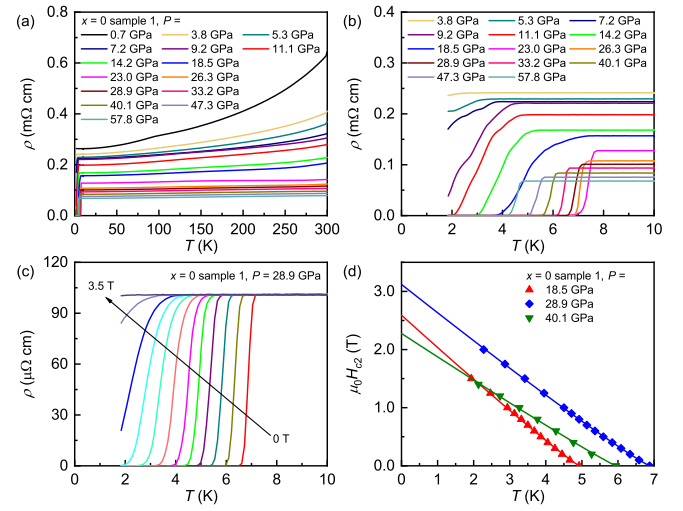


FIG. 2. (a) Temperature dependence of resistivity  $\rho(T)$  at pressures ranging from 0.7 to 57.8 GPa in  $\text{Ge}_2\text{Bi}_2\text{Te}_5$  ( $x = 0$ , sample 1). (b) The enlarged  $\rho(T)$  curves below 10 K. (c) The  $\rho(T)$  as a function of temperature under various magnetic fields at 28.9 GPa. (d) The temperature dependence of upper critical field  $\mu_0 H_{c2}(T)$  at 18.5, 28.9 and 40.1 GPa, respectively. The solid lines represent the fitting results using the equation  $\mu_0 H_{c2}(T) = \mu_0 H_{c2}(0)(1 - (T/T_c))^{1+\alpha}$ .

the similar superconducting phenomena, as depicted in Figs. S2(a) and S2(b) [65]. To gain further insight into the superconducting state, the  $\rho(T)$  curves under different magnetic fields at representative pressures were measured (Figs. 2(c), S3(a) and S3(b) [65]). For  $P = 28.9$  GPa (Fig. 2(c)), the  $T_{c,\text{onset}}$  is gradually suppressed with increasing field and it can not be observed above 2 K when  $\mu_0 H = 3.5$  T. Using the criterion of 50 % normal state resistivity just above  $T_{c,\text{onset}}$ , the temperature dependence of upper critical field  $\mu_0 H_{c2}(T)$  at selected pressures can be extracted, as shown in Fig. 2(d). The  $\mu_0 H_{c2}(T) = \mu_0 H_{c2}(0)(1 - (T/T_c))^{1+\alpha}$  equation [66] is used to fit these curves, where  $\mu_0 H_{c2}(0)$  represents the upper critical field at 0 K. The fitted value of  $\mu_0 H_{c2}(0)$  are 2.59(3) T for 18.5 GPa, 3.12(2) T for 28.9 GPa and 2.28(5) T for 40.1 GPa, respectively. As the Pauli limiting field  $\mu_0 H_P(0)$  ( $= 1.86 T_c$ )  $\sim 9.15$  T – 11.05 T, which are larger than above values of  $\mu_0 H_{c2}(0)$ , it suggests that the orbital-depairing mechanism should be dominant.

We now turn to the pressure effects on the Mn doped  $\text{Ge}_2\text{Bi}_2\text{Te}_5$  single crystals. For  $x = 0.25$  sample (Figs. 3(a) and 3(b)), the values of  $\rho(T)$  initially decrease dramatically as pressure increases. Then the  $\rho(T)$  curve exhibits a metallic behavior in the whole temperature range at the pressure of 19.5 GPa. Simultaneously, the  $\rho(T)$  curve drops slightly at  $T_{c,\text{onset}} \sim 2.3$  K. Upon further compression, the values of normal-state  $\rho(T)$  decline slowly and the drop becomes more dramatic while  $T_{c,\text{onset}}$  remains almost unchanged. When the pressure is applied at 42.2 GPa,  $T_{c,\text{onset}}$  is about 2.26 K and the  $T_{c,\text{zero}}$  is detected at approximately 1.84 K. When the

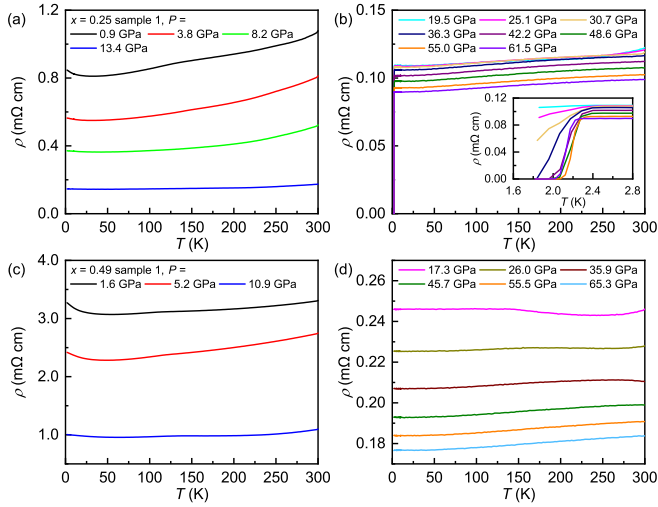


FIG. 3. (a) and (b) Temperature dependence of  $\rho(T)$  under pressures up to 61.5 GPa for  $x = 0.25$  sample. The inset of (b) shows the enlarged  $\rho(T)$  curves from 1.8 to 4 K. (c) and (d) The  $\rho(T)$  curves in the pressure range from 1.6 to 65.3 GPa for  $x = 0.49$  sample.

pressure is further increased to 61.5 GPa, both  $T_{c,\text{onset}}$  and  $T_{c,\text{zero}}$  present slight variations, reaching  $\sim 2.20$  K and 1.97 K at 61.5 GPa, respectively. Furthermore, the temperature dependence of  $\rho(T)$  under various magnetic fields at a pressure of 55.0 GPa is depicted in Fig. S4(a) [65]. It can be seen that the SC is suppressed quickly by applying only a small field of 0.3 T, which is much smaller than that in undoped  $\text{Ge}_2\text{Bi}_2\text{Te}_5$ . The  $\mu_0 H_{c2}(T)$  curve can also be described by the equation  $\mu_0 H_{c2}(T) = \mu_0 H_{c2}(0)(1 - (T/T_c))^{1+\alpha}$ , and the fitted  $\mu_0 H_{c2}(0)$  is 1.14(6) T, confirming the dramatically decrease of  $\mu_0 H_{c2}(0)$  with Mn doping. By contrast, the highly doped sample with  $x = 0.49$  also exhibits the analogous resistivity behavior under high pressure, as illustrated in Figs. 3(c) and 3(d). The values of  $\rho(T)$  is suppressed by one order of magnitude when the pressure approaches 65.3 GPa. Nevertheless, distinct from the samples with  $x = 0$  and 0.25, no superconducting transition appears in our measured pressure range. Additionally, the transport behaviors under pressure of  $x = 0.25$  and 0.49 samples can be reproduced, as presented in Figs. S5 and S6 [65].

We summarized the electronic phase diagram of  $(\text{Ge}_{1-x}\text{Mn}_x)_2\text{Bi}_2\text{Te}_5$  with the variations of pressure and  $x$  (Fig. 4). For  $\text{Ge}_2\text{Bi}_2\text{Te}_5$ , which is paramagnetic at ambient pressure, the pressure dependence of  $T_c$  shows a dome-shaped feature. SC emerges above  $\sim 4$  GPa, boosts to the maximum value of 7.6 K at 23.0 GPa and then decreases with increasing pressure further. For  $x = 0.25$  sample with  $T_N \sim 6$  K, superconducting region is significantly narrowed. The pressure exceeding 19 GPa is required to induce SC, and the  $T_c$  forms a plateau at approximately 2.3 K over a wide pressure range from 20 to 60 GPa. In the case of higher Mn doped sample ( $x =$

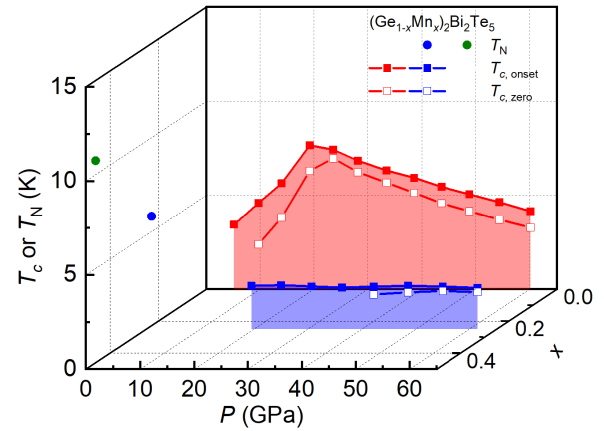


FIG. 4. Electronic phase diagram of  $(\text{Ge}_{1-x}\text{Mn}_x)_2\text{Bi}_2\text{Te}_5$  ( $x = 0, 0.25$  and 0.49).

0.49) with higher  $T_N \sim 12$  K, SC is further suppressed, which can not be observed up to the maximum pressure of 65 GPa. These results suggest that AFM order and SC are competitive each other, indicating that magnetic interaction may have adverse effects on the formation of Cooper pairs in  $(\text{Ge}_{1-x}\text{Mn}_x)_2\text{Bi}_2\text{Te}_5$ .

Finally, we summarize the pressure-induced SC in  $(\text{Ge}_{1-x}\text{Mn}_x)_2\text{Bi}_2\text{Te}_5$  and other members of the  $mAX \cdot nB_2X_3$  family in Table I, including both magnetic and non-magnetic systems. Among the non-magnetic members, those  $B_2X_3$  and  $AX \cdot nB_2X_3$  phases exhibit SC under pressure. Notably, we report here the first observation of pressure-induced SC among  $2AX \cdot B_2X_3$ -type materials. Strikingly, the maximum  $T_c$  across these systems are very similar, falling in the range of 6.3 – 8.5 K, although the required pressures vary considerably, from about 8 to 34 GPa. This suggests that pressure-induced SC in the  $mAX \cdot nB_2X_3$  family may share a common underlying origin or mechanism. It is noted that In-doped  $\text{SnBi}_2\text{Te}_4$  and  $\text{PbBi}_2\text{Te}_4$  exhibit SC even at ambient pressure although the  $T_c$  is rather low ( $\sim 2$  K). It would be interesting to explore the evolution of SC under pressure in these systems. As for magnetic members,  $\text{MnSb}_4\text{Te}_7$  is the only one hosting pressure-induced SC reported in the literature. Our present work establishes that applying pressure to  $\text{Ge}_2\text{Bi}_2\text{Te}_5$  with low Mn-doping levels can trigger a transition from an AFM ground state at ambient pressure to a superconducting state, thereby adding a new magnetic member to this category. Moreover, the  $T_c$  of  $x = 0.25$  sample is only about 2 K, similar to that of  $\text{MnSb}_4\text{Te}_7$ , and both of them have comparable  $T_{Ns}$ . It implies that there is a competing relationship between AFM and SC, and magnetic interactions in these systems may have a similar depairing effect on SC.

TABLE I. SC induced by pressure or chemical doping in pseudobinary chalcogenides  $mAX \cdot nB_2X_3$  ( $A = \text{Ge, Sn, Pb, Mn}$ ;  $B = \text{Sb, Bi}$ ;  $X = \text{Se, Te}$ ), along with their maximum  $T_c$  values. Here, “ $\times$ ” indicates no SC observed above 2 K, while “/” denotes no relevant reports.

Nonmagnetic	Maximum $T_c$	Reference	Magnetic	Maximum $T_c$	Reference
$\text{Ge}_2\text{Bi}_2\text{Te}_5$	~7.6 K at 23.0 GPa	This work	$(\text{Ge}_{1-x}\text{Mn}_x)_2\text{Bi}_2\text{Te}_5$ ( $x = 0.25$ ) $(\text{Ge}_{1-x}\text{Mn}_x)_2\text{Bi}_2\text{Te}_5$ ( $x = 0.49$ )	2.3 K at 55.0 GPa $\times$	This work This work
$\text{GeBi}_2\text{Te}_4$	~8.4 K at 14.6 GPa	[52]	$\text{MnBi}_2\text{Te}_4$	$\times$	[67]
$\text{GeBi}_4\text{Te}_7$	~8.3 K at 20.0 GPa	[?]	$\text{MnBi}_4\text{Te}_7$	$\times$	[67, 68]
$\text{GeSb}_2\text{Te}_4$	~8 K at 22 GPa	[54]	$\text{MnSb}_2\text{Te}_4$	$\times$	[69]
$\text{GeSb}_4\text{Te}_7$	~8 K at 34 GPa	[55]	$\text{MnSb}_4\text{Te}_7$	~2.2 K at 50.7 GPa	[58]
$\text{SnBi}_2\text{Te}_4$	~8.5 K at 22 GPa	[56]	$\text{MnBi}_6\text{Te}_{10}$	$\times$	[68]
$\text{SnSb}_2\text{Te}_4$	~7.4 K at 33 GPa	[57]	$\text{MnSb}_6\text{Te}_{10}$	/	
$\text{Bi}_2\text{Se}_3$	~7 K at 30 GPa	[48]			
$\text{Bi}_2\text{Te}_3$	~8 K at 9 GPa	[49]			
$\text{Sb}_2\text{Te}_3$	~6.3 K at 7.5 GPa	[70]			
$\text{BiTe}$	~8.4 K at 11.9 GPa	[71]			
$\text{Sn}_{1-x}\text{In}_x\text{Bi}_2\text{Te}_4$	~1.8 K for $x = 0.6$	[50]			
$\text{Pb}_{1-x}\text{In}_x\text{Bi}_2\text{Te}_4$	~2.1 K for $x = 0.7$	[51]			

#### IV. CONCLUSION

In summary, we discovered the pressure-induced SC in non-magnetic TI  $\text{Ge}_2\text{Bi}_2\text{Te}_5$  with its  $T_c$  following a dome-shaped evolution as a function of pressure. Furthermore, the introduction of Mn doping leads to the emergence of AFM order at ambient pressure and strongly suppresses the  $T_c$  of pressure-induced SC. Similar behaviors have been observed in  $\text{GeSb}_4\text{Te}_7$  and  $\text{MnSb}_4\text{Te}_7$ . It suggests that within this family of topological materials, magnetic interactions appear to be detrimental to the formation of SC. Present study provides experimental insights for a deeper understanding of the relationship between band topology, magnetism, and SC in  $mAX \cdot nB_2X_3$  material family. It also offers a new material platform for exploring TSC and correlated topological states.

<sup>†</sup> These authors contributed equally to this work.

<sup>\*</sup> Corresponding authors: X. Z. (zhangxiaobupt@bupt.edu.cn), Y. P. Q. (qiyp@shanghaitech.edu.cn), H. C. L. (hlei@ruc.edu.cn), S. G. W. (sgwang@ahu.edu.cn)

#### ACKNOWLEDGMENTS

This work was supported by the National Key R&D Program of China (Grants No. 2022YFA1403800, 2023YFA1406500 and 2023YFA1607400), the National Natural Science Foundation of China (Grants No. 12274459, 52130103 and 52572288), and the China Postdoctoral Science Foundation (Grant No. 2023M730011).

---

[1] L. Fu, C. L. Kane, and E. J. Mele, Topological insulators in three dimensions, *Phys. Rev. Lett.* **98**, 106803 (2007).

[2] M. Z. Hasan and C. L. Kane, Colloquium: Topological insulators, *Rev. Mod. Phys.* **82**, 3045 (2010).

[3] X.-L. Qi and S.-C. Zhang, Topological insulators and superconductors, *Rev. Mod. Phys.* **83**, 1057 (2011).

[4] B. Yan and S.-C. Zhang, Topological materials, *Rep. Prog. Phys.* **75**, 096501 (2012).

[5] Y. Ando, Topological insulator materials, *J. Phys. Soc. Jpn.* **82**, 102001 (2013).

[6] Y. Tokura, K. Yasuda, and A. Tsukazaki, Magnetic topological insulators, *Nat. Rev. Phys.* **1**, 126 (2019).

[7] K. He, Y. Wang, and Q.-K. Xue, Topological materials: Quantum anomalous hall system, *Annu. Rev. Condens. Matter Phys.* **9**, 329 (2018).

[8] C.-X. Liu, S.-C. Zhang, and X.-L. Qi, The quantum anomalous hall effect: Theory and experiment, *Annu. Rev. Condens. Matter Phys.* **7**, 301 (2016).

[9] J. Wang, B. Lian, X.-L. Qi, and S.-C. Zhang, Quantized topological magnetoelectric effect of the zero-plateau quantum anomalous hall state, *Phys. Rev. B* **92**, 081107 (2015).

[10] X.-L. Qi, T. L. Hughes, and S.-C. Zhang, Topological field theory of time-reversal invariant insulators, *Phys. Rev. B* **78**, 195424 (2008).

[11] R. S. K. Mong, A. M. Essin, and J. E. Moore, Antiferromagnetic topological insulators, *Phys. Rev. B* **81**, 245209 (2010).

[12] C.-Z. Chang, J. Zhang, X. Feng, J. Shen, Z. Zhang, M. Guo, K. Li, Y. Ou, P. Wei, L.-L. Wang, Z.-Q. Ji, Y. Feng, S. Ji, X. Chen, J. Jia, X. Dai, Z. Fang, S.-C. Zhang, K. He, Y. Wang, L. Lu, X.-C. Ma, and Q.-K. Xue, Experimental observation of the quantum anomalous hall effect in a magnetic topological insulator, *Science* **340**,

167 (2013).

[13] J. Li, Y. Li, S. Du, Z. Wang, B.-L. Gu, S.-C. Zhang, K. He, W. Duan, and Y. Xu, Intrinsic magnetic topological insulators in van der waals layered  $MnBi_2Te_4$ -family materials, *Sci. Adv.* **5**, eaaw5685 (2019).

[14] S. R. Elliott and M. Franz, Colloquium: Majorana fermions in nuclear, particle, and solid-state physics, *Rev. Mod. Phys.* **87**, 137 (2015).

[15] X.-L. Qi, T. L. Hughes, S. Raghu, and S.-C. Zhang, Time-reversal-invariant topological superconductors and superfluids in two and three dimensions, *Phys. Rev. Lett.* **102**, 187001 (2009).

[16] L. Fu and C. L. Kane, Superconducting proximity effect and majorana fermions at the surface of a topological insulator, *Phys. Rev. Lett.* **100**, 096407 (2008).

[17] A. P. Schnyder, S. Ryu, A. Furusaki, and A. W. W. Ludwig, Classification of topological insulators and superconductors in three spatial dimensions, *Phys. Rev. B* **78**, 195125 (2008).

[18] S. Ryu, A. P. Schnyder, A. Furusaki, and A. W. W. Ludwig, Topological insulators and superconductors: tenfold way and dimensional hierarchy, *New J. Phys.* **12**, 065010 (2010).

[19] A. R. Akhmerov, J. Nilsson, and C. W. J. Beenakker, Electrically detected interferometry of majorana fermions in a topological insulator, *Phys. Rev. Lett.* **102**, 216404 (2009).

[20] F. Wilczek, Majorana returns, *Nat. Phys.* **5**, 614 (2009).

[21] C. Nayak, S. H. Simon, A. Stern, M. Freedman, and S. Das Sarma, Non-abelian anyons and topological quantum computation, *Rev. Mod. Phys.* **80**, 1083 (2008).

[22] D. Wang, L. Kong, P. Fan, H. Chen, S. Zhu, W. Liu, L. Cao, Y. Sun, S. Du, J. Schneeloch, R. Zhong, G. Gu, L. Fu, H. Ding, and H.-J. Gao, Evidence for majorana bound states in an iron-based superconductor, *Science* **362**, 333 (2018).

[23] B. Bradlyn, L. Elcoro, J. Cano, M. G. Vergniory, Z. Wang, C. Felser, M. I. Aroyo, and B. A. Bernevig, Topological quantum chemistry, *Nature* **547**, 298 (2017).

[24] M. G. Vergniory, L. Elcoro, C. Felser, N. Regnault, B. A. Bernevig, and Z. Wang, A complete catalogue of high-quality topological materials, *Nature* **566**, 480 (2019).

[25] M. G. Vergniory, B. J. Wieder, L. Elcoro, S. S. P. Parkin, C. Felser, B. A. Bernevig, and N. Regnault, All topological bands of all nonmagnetic stoichiometric materials, *Science* **376**, eaabg9094 (2022).

[26] M. Nurmamat, K. Okamoto, S. Zhu, T. V. Menshchikova, I. P. Rusinov, V. O. Korostelev, K. Miyamoto, T. Okuda, T. Miyashita, X. Wang, Y. Ishida, K. Sumida, E. F. Schwier, M. Ye, Z. S. Aliev, M. B. Babanly, I. R. Amiraslanov, E. V. Chulkov, K. A. Kokh, O. E. Tereshchenko, K. Shimada, S. Shin, and A. Kimura, Topologically Nontrivial Phase-Change Compound  $GeSb_2Te_4$ , *ACS Nano* **14**, 9059 (2020).

[27] K. Okamoto, K. Kuroda, H. Miyahara, K. Miyamoto, T. Okuda, Z. S. Aliev, M. B. Babanly, I. R. Amiraslanov, K. Shimada, H. Namatame, M. Taniguchi, D. A. Samorokov, T. V. Menshchikova, E. V. Chulkov, and A. Kimura, Observation of a highly spin-polarized topological surface state in  $GeBi_2Te_4$ , *Phys. Rev. B* **86**, 195304 (2012).

[28] M. Neupane, S. Y. Xu, L. A. Wray, A. Petersen, R. Shankar, N. Alidoust, C. Liu, A. Fedorov, H. Ji, J. M. Allred, Y. S. Hor, T. R. Chang, H. T. Jeng, H. Lin, A. Bansil, R. J. Cava, and M. Z. Hasan, Topological surface states and Dirac point tuning in ternary topological insulators, *Phys. Rev. B* **85**, 235406 (2012).

[29] Y. Li, C. Huang, G. Wang, J. Hu, S. Duan, C. Xu, Q. Lu, Q. Jing, W. Zhang, and D. Qian, Topological Dirac surface states in ternary compounds  $GeBi_2Te_4$ ,  $SnBi_2Te_4$  and  $Sn_{0.571}Bi_{2.286}Se_4$ , *Chin. Phys. B* **30**, 127901 (2021).

[30] D. Niesner, S. Otto, V. Hermann, T. Fauster, T. V. Menshchikova, S. V. Eremeev, Z. S. Aliev, I. R. Amiraslanov, M. B. Babanly, P. M. Echenique, and E. V. Chulkov, Bulk and surface electron dynamics in a *p*-type topological insulator  $SnSb_2Te_4$ , *Phys. Rev. B* **89**, 081404 (2014).

[31] S. Fragkos, L. Baringthon, P. Tsipas, E. Xenogianopoulos, P. Le Fèvre, P. Kumar, H. Okuno, N. Reyren, A. Lemaitre, G. Patriarche, J.-M. George, and A. Dimoulas, Topological surface states in epitaxial  $(SnBi_2Te_4)_n(Bi_2Te_3)_m$  natural van der Waals superlattices, *Phys. Rev. Mater.* **5**, 014203 (2021).

[32] S. Souma, K. Eto, M. Nomura, K. Nakayama, T. Sato, T. Takahashi, K. Segawa, and Y. Ando, Topological Surface States in Lead-Based Ternary Telluride  $Pb(Bi_{1-x}Sb_x)_2Te_4$ , *Phys. Rev. Lett.* **108**, 116801 (2012).

[33] K. Kuroda, H. Miyahara, M. Ye, S. V. Eremeev, Y. M. Koroteev, E. E. Krasovskii, E. V. Chulkov, S. Hiramoto, C. Moriyoshi, Y. Kuroiwa, K. Miyamoto, T. Okuda, M. Arita, K. Shimada, H. Namatame, M. Taniguchi, Y. Ueda, and A. Kimura, Experimental Verification of  $PbBi_2Te_4$  as a 3D Topological Insulator, *Phys. Rev. Lett.* **108**, 206803 (2012).

[34] S. V. Eremeev, G. Landolt, T. V. Menshchikova, B. Slomski, Y. M. Koroteev, Z. S. Aliev, M. B. Babanly, J. Henk, A. Ernst, L. Patthey, A. Eich, A. A. Khajetoorians, J. Hagemeister, O. Pietzsch, J. Wiebe, R. Wiesendanger, P. M. Echenique, S. S. Tsirkin, I. R. Amiraslanov, J. H. Dil, and E. V. Chulkov, Atom-specific spin mapping and buried topological states in a homologous series of topological insulators, *Nat. Commun.* **3**, 635 (2012).

[35] T. Okuda, T. Maegawa, M. Ye, K. Shirai, T. Warashina, K. Miyamoto, K. Kuroda, M. Arita, Z. S. Aliev, I. R. Amiraslanov, M. B. Babanly, E. V. Chulkov, S. V. Eremeev, A. Kimura, H. Namatame, and M. Taniguchi, Experimental Evidence of Hidden Topological Surface States in  $PbBi_4Te_7$ , *Phys. Rev. Lett.* **111**, 206803 (2013).

[36] M. Papagno, S. V. Eremeev, J. Fujii, Z. S. Aliev, M. B. Babanly, S. K. Mahatha, I. Vobornik, N. T. Mamedov, D. Pacilé, and E. V. Chulkov, Multiple Coexisting Dirac Surface States in Three-Dimensional Topological Insulator  $PbBi_6Te_{10}$ , *ACS Nano* **10**, 3518 (2016).

[37] D. Pacilé, S. V. Eremeev, M. Caputo, M. Pisarra, O. De Luca, I. Grimaldi, J. Fujii, Z. S. Aliev, M. B. Babanly, I. Vobornik, R. G. Agostino, A. Goldoni, E. V. Chulkov, and M. Papagno, Deep Insight Into the Electronic Structure of Ternary Topological Insulators: A Comparative Study of  $PbBi_4Te_7$  and  $PbBi_6Te_{10}$ , *Phys. Status. Solidi.-R* **12**, 1800341 (2018).

[38] D. Zhang, M. Shi, T. Zhu, D. Xing, H. Zhang, and J. Wang, Topological Axion States in the Magnetic Insulator  $MnBi_2Te_4$  with the Quantized Magnetoelectric Effect, *Phys. Rev. Lett.* **122**, 206401 (2019).

[39] M. M. Otkrov, I. I. Klimovskikh, H. Bentmann, D. Estyulin, A. Zeugner, Z. S. Aliev, S. Gaß, A. U. B. Wolter, A. V. Koroleva, A. M. Shikin, M. Blanco-Rey, M. Hoffmann, I. P. Rusinov, A. Y. Vyazovskaya, S. V. Eremeev, Y. M. Koroteev, V. M. Kuznetsov, F. Freyse, J.

Sánchez-Barriga, I. R. Amiraslanov, M. B. Babanly, N. T. Mamedov, N. A. Abdullayev, V. N. Zverev, A. Alfonsov, V. Kataev, B. Büchner, E. F. Schwier, S. Kumar, A. Kimura, L. Petaccia, G. Di Santo, R. C. Vidal, S. Schatz, K. Kißner, M. Ünzelmann, C. H. Min, S. Moser, T. R. F. Peixoto, F. Reinert, A. Ernst, P. M. Echenique, A. Isaeva, and E. V. Chulkov, Prediction and observation of an antiferromagnetic topological insulator, *Nature* **576**, 416 (2019).

[40] Y. Gong, J. Guo, J. Li, K. Zhu, M. Liao, X. Liu, Q. Zhang, L. Gu, L. Tang, X. Feng, D. Zhang, W. Li, C. Song, L. Wang, P. Yu, X. Chen, Y. Wang, H. Yao, W. Duan, Y. Xu, S.-C. Zhang, X. Ma, Q.-K. Xue, and K. He, Experimental Realization of an Intrinsic Magnetic Topological Insulator, *Chin. Phys. Lett.* **36**, 076801 (2019).

[41] Y.-J. Hao, P. Liu, Y. Feng, X.-M. Ma, E. F. Schwier, M. Arita, S. Kumar, C. Hu, R. Lu, M. Zeng, Y. Wang, Z. Hao, H.-Y. Sun, K. Zhang, J. Mei, N. Ni, L. Wu, K. Shimada, C. Chen, Q. Liu, and C. Liu, Gapless Surface Dirac Cone in Antiferromagnetic Topological Insulator  $MnBi_2Te_4$ , *Phys. Rev. X* **9**, 041038 (2019).

[42] Y. J. Chen, L. X. Xu, J. H. Li, Y. W. Li, H. Y. Wang, C. F. Zhang, H. Li, Y. Wu, A. J. Liang, C. Chen, S. W. Jung, C. Cacho, Y. H. Mao, S. Liu, M. X. Wang, Y. F. Guo, Y. Xu, Z. K. Liu, L. X. Yang, and Y. L. Chen, Topological Electronic Structure and Its Temperature Evolution in Antiferromagnetic Topological Insulator  $MnBi_2Te_4$ , *Phys. Rev. X* **9**, 041040 (2019).

[43] J. Li, Y. Li, S. Du, Z. Wang, B.-L. Gu, S.-C. Zhang, K. He, W. Duan, and Y. Xu, Intrinsic magnetic topological insulators in van der Waals layered  $MnBi_2Te_4$ -family materials, *Sci. Adv.* **5**, eaaw5685 (2019).

[44] B. Sa, J. Zhou, Z. Sun, J. Tominaga, and R. Ahuja, Topological Insulating in  $GeTe/Sb_2Te_3$  Phase-Change Superlattice, *Phys. Rev. Lett.* **109**, 096802 (2012).

[45] J. Kim, J. Kim, K.-S. Kim, and S.-H. Jhi, Topological phase transition in the interaction of surface dirac fermions in heterostructures, *Phys. Rev. Lett.* **109**, 146601 (2012).

[46] Y. Li, Y. Jia, B. Zhao, H. Bao, H. Huan, H. Weng, and Z. Yang, Stacking-layer-tuned topological phases in  $M_2Bi_2Te_5$  ( $M = Ge, Sn, Pb$ ) films, *Phys. Rev. B* **108**, 085428 (2023).

[47] L. Gao, J. Wu, M. Xi, C. Pei, Q. Wang, Y. Zhao, S. Tian, C. Li, W. Cao, Y. Chen, H. Lei, and Y. Qi, Pressure-tunable magnetic topological phases in magnetic topological insulator  $MnSb_4Te_7$ , *App. Phys. Lett.* **122**, 172404 (2023).

[48] K. Kirshenbaum, P. S. Syers, A. P. Hope, N. P. Butch, J. R. Jeffries, S. T. Weir, J. J. Hamlin, M. B. Maple, Y. K. Vohra, and J. Paglione, Pressure-induced unconventional superconducting phase in the topological insulator  $Bi_2Se_3$ , *Phys. Rev. Lett.* **111**, 087001 (2013).

[49] J. L. Zhang, S. J. Zhang, H. M. Weng, W. Zhang, L. X. Yang, Q. Q. Liu, S. M. Feng, X. C. Wang, R. C. Yu, L. Z. Cao, L. Wang, W. G. Yang, H. Z. Liu, W. Y. Zhao, S. C. Zhang, X. Dai, Z. Fang, and C. Q. Jin, Pressure-induced superconductivity in topological parent compound  $Bi_2Te_3$ , *PNAS* **108**, 24 (2011).

[50] M. A. McGuire, H. Zhang, A. F. May, S. Okamoto, R. G. Moore, X. Wang, C. Girod, S. M. Thomas, F. Ronning, and J. Yan, Superconductivity by alloying the topological insulator  $SnBi_2Te_4$ , *Phys. Rev. Mater.* **7**, 034802 (2023).

[51] X. Xu, D. Ni, W. Xie, and R. J. Cava, Superconductivity in electron-doped  $PbBi_2Te_4$ , *Phys. Rev. B* **108**, 054525 (2023).

[52] C. Liu, Y. Gao, C. Tian, C. Jiang, C. Zhu, X. Wu, X. Huang, and T. Cui, Pressure-driven dome-shaped superconductivity in topological insulator  $GeBi_2Te_4$ , *J. Phys. Condens. Matter* **36**, 225703 (2024).

[53] Y. Huang, N. Zuo, Z. Zhang, C. Xu, X. Xing, W.-H. Jiao, B. Li, W. Zhou, X. Liu, D. Qian, and X. Xu, Pressure-driven superconductivity in the topological insulator  $GeBi_4Te_7$ , *Phys. Rev. B* **112**, 014515 (2025).

[54] E. Greenberg, B. Hen, S. Layek, I. Pozin, R. Friedman, V. Shelukhin, Y. Rosenberg, M. Karpovski, M. P. Pasternak, E. Sterer, Y. Dagan, G. K. Rozenberg, and A. Palevski, Superconductivity in multiple phases of compressed  $GeSb_2Te_4$ , *Phys. Rev. B* **95**, 064514 (2017).

[55] W. Zhou, B. Li, Y. Shen, J. J. Feng, C. Q. Xu, H. T. Guo, Z. He, B. Qian, Z. Zhu, and X. Xu, Multiple superconducting phases driven by pressure in the topological insulator  $GeSb_4Te_7$ , *Phys. Rev. B* **108**, 184504 (2023).

[56] R. Li, G. Liu, Q. Jing, X. Wang, H. Wang, J. Zhang, and Y. Ma, Pressure-induced superconductivity and structural transitions in topological insulator  $SnBi_2Te_4$ , *J. Alloy. Compd.* **900**, 163371 (2022).

[57] P. Song, R. Matsumoto, Z. Hou, S. Adachi, H. Hara, Y. Saito, P. B. Castro, H. Takeya, and Y. Takano, Pressure-induced superconductivity in  $SnSb_2Te_4$ , *J. Phys. Condens. Matter* **32**, 235901 (2020).

[58] C. Pei, M. Xi, Q. Wang, W. Shi, J. Wu, L. Gao, Y. Zhao, S. Tian, W. Cao, C. Li, M. Zhang, S. Zhu, Y. Chen, H. Lei, and Y. Qi, Pressure-induced superconductivity in magnetic topological insulator candidate  $MnSb_4Te_7$ , *Phys. Rev. Mater.* **6**, L101801 (2022).

[59] S. Tian, Y. Zhang, C. Liang, Y. Cao, W. Lv, X. Lv, Z. Wang, T. Qian, H. Lei, and S. Wang, Three-dimensional topological insulator feature of ternary chalcogenide  $Ge_2Bi_2Te_5$ , arXiv: 2601.11339 (2026).

[60] T. Qian, C. Hu, J. Green, E. Feng, H. Cao, and N. Ni, Single crystal growth, chemical defects, magnetic and transport properties of antiferromagnetic topological insulators  $(Ge_{1-\delta-x}Mn_x)_2Bi_2Te_5$  ( $x \leq 0.47$ ,  $0.11 \leq \delta \leq 0.20$ ), *Phys. Rev. Mater.* **8**, 084203 (2024).

[61] H. K. Mao, J. Xu, and P. M. Bell, Calibration of the ruby pressure gauge to 800 kbar under quasi-hydrostatic conditions, *J. Geophys. Res.* **91**, 4673 (1986).

[62] L. E. Shelimova, O. G. Karpinskii, V. S. Zemskov, and P. P. Konstantinov, Structural and electrical properties of layered tetradymite-like compounds in the  $GeTe-Bi_2Te_3$  and  $GeTe-Sb_2Te_3$  systems, *Inorg. Mater.* **36**, 235 (2000).

[63] O. G. Karpinskii, L. E. Shelimova, M. A. Kretova, and V. S. Zemskov, X-ray diffraction study of  $Ge-Bi-Te$  mixed-layer ternary compounds, *Inorg. Mater.* **36**, 1108 (2000).

[64] T. M. Alakbarova, H.-J. Meyer, E. N. Orujiu, I. R. Amiraslanov, and M. B. Babanly, Phase equilibria of the  $GeTe-Bi_2Te_3$  quasi-binary system in the range 0-50  $Bi_2Te_3$ , *Phase Transf.* **94**, 366 (2021).

[65] See Supplemental Material.

[66] K. H. Müller, G. Fuchs, A. Handstein, K. Nenkov, V. N. Narozhnyi, and D. Eckert, The upper critical field in superconducting  $MgB_2$ , *J. Alloy. Compd.* **322**, L10 (2001).

[67] C. Pei, Y. Xia, J. Wu, Y. Zhao, L. Gao, T. Ying, B. Gao, N. Li, W. Yang, D. Zhang, H. Gou, Y. Chen, H. Hosono, G. Li, and Y. Qi, Pressure-Induced Topological and Structural Phase Transitions in an Antiferromagnetic

netic Topological Insulator, *Chin. Phys. Lett.* **37**, 066401 (2020).

[68] J. Shao, Y. Liu, M. Zeng, J. Li, X. Wu, X.-M. Ma, F. Jin, R. Lu, Y. Sun, M. Gu, K. Wang, W. Wu, L. Wu, C. Liu, Q. Liu, and Y. Zhao, Pressure-tuned intralayer exchange in superlattice-like  $\text{MnBi}_2\text{Te}_4/(\text{Bi}_2\text{Te}_3)_n$  topological insulators, *Nano Lett.* **21**, 5874 (2021).

[69] Y. Yin, X. Ma, D. Yan, C. Yi, B. Yue, J. Dai, L. Zhao, X. Yu, Y. Shi, J.-T. Wang, and F. Hong, Pressure-driven electronic and structural phase transition in intrinsic magnetic topological insulator  $\text{MnSb}_2\text{Te}_4$ , *Phys. Rev. B* **104**, 174114 (2021).

[70] J. Zhu, J. L. Zhang, P. P. Kong, S. J. Zhang, X. H. Yu, J. L. Zhu, Q. Q. Liu, X. Li, R. C. Yu, R. Ahuja, W. G. Yang, G. Y. Shen, H. K. Mao, H. M. Weng, X. Dai, Z. Fang, Y. S. Zhao, and C. Q. Jin, Superconductivity in topological insulator  $\text{Sb}_2\text{Te}_3$  induced by pressure, *Sci. Rep.* **3**, 2016 (2013).

[71] S. Zhu, B. Zhu, C. Pei, Q. Wang, J. Chen, Q. Zhang, T. Ying, L. Gu, Y. Zhao, C. Li, W. Cao, M. Zhang, L. Zhang, J. Sun, Y. Chen, J. Wu, and Y. Qi, Distinct superconducting states in the pressure-induced metallic structures of topological heterostructure BiTe, *Mater. Today Phys.* **42**, 101377 (2024).